Activity Calculation and Vacuum Separation Theoretical Research concerning Ag–Cu, Ag–Sb and Cu–Sb Binary Alloys

Qingsong Li [1,2,3], Yang Tian [1,2,3,4,*], Lingxin Kong [1,2,3,4], Bin Yang [1,2,3,4], Baoqiang Xu [1,2,3,4], Wenlong Jiang [1,2,3,4] and Lipeng Wang [1,2,3]

1 Key Laboratory for Nonferrous Vacuum Metallurgy of Yunnan Province, Kunming University of Science and Technology, Kunming 650093, China; qingsong_li_2024@126.com (Q.L.); kkmust@126.com (L.K.); kgyb2005@126.com (B.Y.); kmxbq@126.com (B.X.); wenlong_jiang@kust.edu.cn (W.J.)
2 National Engineering Research Center of Vacuum Metallurgy, Kunming University of Science and Technology, Kunming 650093, China
3 Faculty of Metallurgical and Energy Engineering, Kunming University of Science and Technology, Kunming 650093, China
4 State Key Laboratory of Complex Nonferrous Metal Resources Clean Utilization, Kunming University of Science and Technology, Kunming 650093, China
* Correspondence: emontian@hotmail.com; Tel.: +86-13888805314

Abstract: The Ag–Cu–Sb system is a key component of lead anode slime and boasts an exceptionally high economic recovery value. In this work, six models, including the Molecular Interaction Volume Model (MIVM), Modified Molecular Interaction Volume Model (M-MIVM), Wilson equation, Miedema model, Regular Solution Model (RSE) and Sub-Regular Solution Model (SRSE), are used to calculate the predicted values of the activity and its deviations with experimental data for binary alloys in the Ag–Cu–Sb system for the first time. The result reveals that the overall means of the average relative deviation and average standard deviation of the M-MIVM are 0.01501 and 3.97278%, respectively, which are about two to six times smaller than those of the other five models, indicating the stability and reliability of the M-MIVM. In the meantime, the predicted data of the Cu–Ag binary alloy at 1423 K, Sb–Ag binary alloy at 1250 K and Sb–Cu binary alloy at 1375 K calculated from the M-MIVM are more reliable and pass the Herington test. Then, the separation coefficient–composition (β–x), temperature–composition (T–x–y) and pressure–composition (P–x–y) of the Cu–Ag, Sb–Ag and Sb–Cu binary alloys are plotted based on the M-MIVM and vacuum theories, showing that the Cu–Ag binary alloy is relatively difficult to separate and that high temperatures or high copper contents are detrimental to obtaining high-purity silver. Meanwhile, theoretical data of the T–x–y diagram are consistent with the available experimental data. These results can guide vacuum separation experiments and industrial production concerning Ag–Cu, Ag–Sb and Cu–Sb binary alloys.

Keywords: Ag–Cu–Sb system; activity and activity coefficient; M-MIVM; T–x–y diagram; vacuum separation

1. Introduction

Silver and gold metals boast the unique and excellent properties of corrosion resistance, stability, ductility, conductivity, and thermal conductivity [1,2] and play a significant role in high-tech territory such as electronics, communication, aerospace and optoelectronics [3,4]. In the recovery of silver or gold from minerals, copper anode slime and lead anode slime, it is inevitable to form the Ag–Au system, which always contains Cu and Sb metals [5,6], because the physical and chemical properties of Ag, Au, Cu and Sb metals are similar. The methods for the separation of Ag and Au from the Ag–Au system mainly involve chemical and electrolytic approaches, but these often have some problems, such as the low leaching rate due to the mutual encapsulation of silver and gold and the abundant accumulation of silver or gold pure metal in an electrolytic manner [7], high acid consumption and

environmentally unfriendliness caused by nitrogen oxides in the chemical method [8]. In the past few years, much attention has been paid to the vacuum approach due to its advantages of a short flow [9], high efficiency [10], the kindness to the environment and so forth. Khlebnikov [11] used the vacuum technology to separate the Ag–Au binary alloy, obtaining crude silver with a purity of 93% and crude gold with a purity of 95%. Our research group has carried out a series of experimental studies on the separation of Ag and Au from Ag–Au [12], Ag–Au–Sb, Ag–Au–Cu [13] and Ag–Au–Cu–Sb [14] alloys in this manner, albeit separately. These results revealed that Ag and Au can be effectively separated, with Ag enriched in the gas phase and Au enriched in the liquid phase. The recoveries of Ag and Au were all above 99%, with less than 200 g/t gold in the crude silver and less than 10% silver in the crude gold. However, there are few thermodynamic studies on separating the Ag–Au system by this method. Wang [12,13] reported thermodynamic research on the vacuum separation of Ag–Au and Ag–Cu–Au alloys, while other alloys in the system haven't been reported. In the meantime, they found that the masses of the Ag–Cu–Sb alloy cannot be ignored in the process of forming the Ag–Au system. However, accurate data concerning the activity or activity coefficient are first needed for thermodynamic investigations [15].

To date, the study of the activity of the Ag–Cu–Sb system is rare, and in extraordinary cases, the experimental activity values of the Ag–Cu–Sb ternary alloy have failed to be found, thus there is an urgent need for activity research to fill the gap in this field. Furthermore, because of the challenging operation, high cost and inaccurate activity values due to the high temperature condition in experimental measurements [16,17], the predictive activity model is the mainstream method of research concerning activity. And the activity study of a ternary alloy is based on the conclusion of an activity study of its binary alloys [18,19]. Meanwhile, Prausnitz [20] divided the "applied model" for the activity study of binary alloys into three kinds: the local composition model, the Wohl model and special model represented by the Miedema model that can directly obtain thermodynamic data based on the physical properties of the alloy itself. The local composition model comprises the MIVM, M-MIVM, Wilson equation and Non-Random Two-Liquid (NRTL) model, which introduces a parameter of unclear physical significance [21], and the Wohl model comprises the RSM, SRSM and others. Based on what has been mentioned above, each model has unique advantages and limitations [22], so researchers usually compute the average relative deviation and the average standard deviation [23] to select the appropriate predictive model for a particular system.

Therefore, in this work, the activity and activity coefficient of the Cu–Ag, Sb–Ag and Sb–Cu binary alloys are projected by the MIVM, M-MIVM, Wilson equation, Miedema model, RSE and SRSE in the first place, and then these predicted values are compared with experimental data (Cu–Ag binary alloy at 1400 K and 1423 K, Sb–Ag binary alloy at 1250 K and 1300 K as well as Sb–Cu binary alloy at 1190 K and 1375 K) [24,25] by deviations in order to select an excellent model that is optimal for the Ag–Cu–Sb ternary alloy. In the second place, the predictive activity is inspected based on the excellent model by means of the thermodynamic consistency. Finally, to update the diagrams of the separation coefficient, the temperature and pressure, respectively, concerning the ingredient are based on the selectively reliable model. This work aims to provide more accurate guidance for the further activity study of the Ag–Cu–Sb ternary alloy and separation of its binary alloys in experiments or industrialized production, perhaps even to lay the foundation for separation research on the Ag–Au system.

2. Method

2.1. Model Induction

2.1.1. MIVM, M-MIVM and Wilson Equation

In 2000, a new model of the thermodynamics of liquid mixtures, the MIVM, was established based on statistical thermodynamics and the fluid-phase equilibrium theory by Tao [26], which regards liquid molecules as performing non-random movements from

one cavity to another in the liquid, thereby not behaving like gas molecules that move randomly or solid molecules that only undergo thermal vibration at lattice points. The expression of the molar excess Gibbs energy G_M^E in a multi-component system is:

$$G_M^E = \sum_{i=1}^{n} x_i \ln \frac{V_{mi}}{\sum_{j=1}^{n} x_j V_{mj} B_{ji}} - \frac{1}{2} \sum_{i=1}^{N} Z_i x_i \left(\frac{\sum_{j=1}^{n} x_j B_{ji} \ln B_{ji}}{\sum_{k=1}^{n} x_k B_{ki}} \right) \tag{1}$$

Combining Formula (1) with $(\partial G_M^E / \partial x_i)_{T,P,i \neq j} = RT \ln \gamma_i$, the binary i–j activity coefficients are:

$$\ln \gamma_i = 1 + \ln \frac{V_{mi}}{x_i V_{mi} + x_j V_{mj} B_{ji}} - \frac{x_i V_{mi}}{x_i V_{mi} + x_j V_{mj} B_{ji}} - \frac{x_j V_{mi} B_{ij}}{x_j V_{mj} + x_i V_{mi} B_{ij}} - \frac{x_j^2}{2} \cdot \left(\frac{B_{ji}^2 Z_i \ln B_{ji}}{(x_i + x_j B_{ji})^2} + \frac{B_{ij} Z_j \ln B_{ij}}{(x_j + x_i B_{ij})^2} \right) \tag{2}$$

$$\ln \gamma_j = 1 + \ln \frac{V_{mj}}{x_j V_{mj} + x_i V_{mi} B_{ij}} - \frac{x_j V_{mj}}{x_j V_{mj} + x_i V_{mi} B_{ij}} - \frac{x_j V_{mi} B_{ij}}{x_i V_{mi} + x_j V_{mj} B_{ji}} - \frac{x_i^2}{2} \cdot \left(\frac{B_{ji} Z_i \ln B_{ji}}{(x_i + x_j B_{ji})^2} + \frac{B_{ij}^2 Z_j \ln B_{ij}}{(x_j + x_i B_{ij})^2} \right) \tag{3}$$

where x_i is the molar fraction; Z_i and Z_j refer to the coordination number of pure solid i and j, respectively, and are defined by Equation (6); V_{mi} is the molar volume at a certain temperature; and B_{ij} is the pair potential energy interaction parameter that is calculated according to Equation (4).

$$B_{ij} = exp \left[-\left(\frac{\varepsilon_{ij} - \varepsilon_{jj}}{kT} \right) \right], B_{ji} = exp \left[-\left(\frac{\varepsilon_{ji} - \varepsilon_{ii}}{kT} \right) \right] \tag{4}$$

where ε_{ij}, ε_{ji}, ε_{ii} and ε_{jj} are the molecular pair potential energy of i–j, j–i, i–i, and j–j, respectively, and are usually considered to be temperature-independent, so that when the pair potential energy interaction parameter (B_{ij}, B_{ji}) is known at a certain temperature, the pair potential energy interaction parameter (B_{ij0}, B_{ji0}) at any temperature can be obtained, like Equation (5) showing the following.

$$T \ln B_{ji} = T_0 \ln B_{ji0}, \ T \ln B_{ij} = T_0 \ln B_{ij0} \tag{5}$$

$$Z_i = \frac{4\sqrt{2\pi}}{3} \left(\frac{r_{mi}^3 - r_{0i}^3}{r_{mi} - r_{0i}} \right) \rho_i r_{mi} exp \left(\frac{\Delta H_{mi}(T_{mi} - T)}{Z_c R T T_{mi}} \right) \tag{6}$$

where r_{0i} and r_{mi} are the initial and first peak values of the radial distance at the melting point, respectively; ΔH_{mi} and T_{mi} are the enthalpy of the fusion and melting point, separately; Z_c is the nearest neighbor coordination number and takes a value of 12; and ρ_i is the density, $\rho_i = 0.6002 / V_{mi}$.

The MIVM has been widely applied in the metallurgical field due to its clear physical meaning and excellent fitting effect, and it can be deduced into the Wilson equation and NRTL under certain conditions. However, there is a loss of advantage for the prediction of the activity of asymmetric systems. In recent times, Dai [27] proposed the M-MIVM based on the Scott's two-fluid and Scatchard–Hildebrand theories. The molar excess Gibbs energy G_M^E of binary alloys is shown as following:

$$\frac{G_m^E}{RT} = -x_i \ln(x_i + x_j \frac{V_{mj}}{V_{mi}} B_{ji}) - x_j \ln(x_j + x_i \frac{V_{mi}}{V_{mj}} B_{ij}) + x_i x_j \left(\frac{A_{ji}}{x_i + x_i \frac{V_{mj}}{V_{mi}} B_{ij}} + \frac{A_{ij}}{x_j + x_j \frac{V_{mi}}{V_{mj}} B_{ji}} \right) \tag{7}$$

$$A_{ji} = K' C_i^0 (\varepsilon_{ji} - \varepsilon_{ii}), A_{ij} = K' C_j^0 (\varepsilon_{ij} - \varepsilon_{ji}) \tag{8}$$

Then

$$K' = \frac{3K}{k} \tag{9}$$

$$B_{ij} = \frac{P_{ij}}{P_{jj}}, B_{ji} = \frac{P_{ji}}{P_{ii}} \tag{10}$$

where A_{ij} and B_{ij} are the volume and energy parameters defined by Equations (8) and (10), respectively; C_i^0 is a proportional constant; K and k are the universal constant independent of the molecular nature and Boltzmann constant, respectively; and P_{ij} is the probability of molecule i arising in the first coordination layer of nuclear molecule j.

The volume parameter B_{ij} is dependent on the temperature, so the B_{ij0} at an arbitrary temperature T_0 can be obtained from Equation (11). Additionally, the energy parameter A_{ij} is also closely bound up with the temperature according to Equation (12).

$$B_{ij0} = exp\left(\frac{T}{T_0}\ln B_{ij}\right), B_{ji0} = exp\left(\frac{T}{T_0}\ln B_{ij}\right) \tag{11}$$

$$A_{ij0} = \frac{T}{T_0}A_{ij}, A_{ji0} = \frac{T}{T_0}A_{ji} \tag{12}$$

Simultaneously, the activity coefficient of i in binary systems can be expressed as:

$$
\ln\gamma_i = -\ln\left(x_i + \frac{V_{mj}}{V_{mi}}B_{ji}x_j\right) - x_i x_j\left[\frac{1-\frac{V_{mj}}{V_{mi}}B_{ji}}{x_i+\frac{V_{mj}}{V_{mi}}B_{ji}x_j}\right] - x_j^2\left[\frac{\frac{V_{mj}}{V_{mj}}B_{ij}-1}{x_j+\frac{V_{mi}}{V_{mj}}B_{ji}x_i}\right] + x_j^2\left[\frac{A_{ji}}{x_i+\frac{V_{mj}}{V_{mi}}B_{ji}x_j} + \frac{A_{ij}}{x_j+\frac{V_{mi}}{V_{mj}}B_{ij}x_i}\right]
$$
$$
- x_i x_j^2\left[\frac{A_{ji}\left(1-\frac{V_{mj}}{V_{mi}}B_{ji}\right)}{\left(x_i+\frac{V_{mj}}{V_{mi}}B_{ji}x_i\right)^2} + \frac{A_{ij}\left(\frac{V_{mi}}{V_{mj}}B_{ij}-1\right)}{\left(x_j+\frac{V_{mi}}{V_{mj}}B_{ij}\right)^2}\right]^2 \tag{13}
$$

Then, the needed data of the Ag, Cu and Sb metals in the MIVM and M-MVIM are provided in Table 1.

Table 1. The related parameters of pure metal in the MVIM and M-MVIM [28]. Reprinted from Ref. [28].

i	V_{mi} (10^{-6} m³/mol)	T_{mi}/K	ΔH_{mi} (kJ/mol)	r_{0i}	r_{mi}
Ag	$11.64(1 + 0.98 \times 10^{-4} \times (T - T_{mi}))$	1234	11.09	2.46	2.89
Cu	$7.99(1 + 1.00 \times 10^{-4} \times (T - T_{mi}))$	1356	13.00	2.15	2.56
Sb	$18.87(1 + 1.3 \times 10^{-4} \times (T - T_{mi}))$	904	39.70	2.57	3.14

When the second term in Equation (1) is equal to zero and $A_{ij} = V_{mj}B_{ji}/V_{mi}$, Equation (1) can be reduced to the Wilson equation and the expression of the molar excess Gibbs energy G_M^E for a multi-component alloy is as follows:

$$\frac{G_m^E}{RT} = -\sum_{i=1}^{k} x_i\ln\left(\sum_{j=1}^{k} x_j\Lambda_{ji}\right) \tag{14}$$

The activity coefficient of i in binary systems is:

$$\ln\gamma_i = -\ln(x_i + x_j\Lambda_{ji}) + x_j\left(\frac{\Lambda_{ji}}{x_i + x_j\Lambda_{ji}} - \frac{\Lambda_{ij}}{x_j + x_i\Lambda_{ij}}\right) \tag{15}$$

$\Lambda_{ij} = \frac{V_{mi}}{V_{mj}}exp\left[-\left(\frac{\lambda_{ij}-\lambda_{jj}}{RT}\right)\right]$ and $\Lambda_{ji} = \frac{V_{mj}}{V_{mi}}exp\left[-\left(\frac{\lambda_{ji}-\lambda_{ii}}{RT}\right)\right]$ are the two main parameters in Equation (15).

2.1.2. Miedema Model

The Miedema model [29], which is semi-empirical, is a significant achievement of alloy theory in recent years. It extends the application scale from pure metals to binary alloys based on the Wigner–Seitz cell theory. For a binary i–j alloy, the activity coefficient of component i can be obtained by the following equation:

$$\ln \gamma_i = \frac{\alpha_{ij}\Delta H_{AB}}{RT}\left[1+(1-x_i)\left[\frac{1}{x_i}-\frac{1}{1-x_i}-\frac{\mu_i(\phi_i-\phi_j)}{1+\mu_i(1-x_i)(\phi_i-\phi_j)}-\frac{\mu_i(\phi_i-\phi_j)}{1+\mu_j(\phi_j-\phi_i)}-\frac{V_{mi}^{2/3}[1+\mu_i(1-2x_i)(\phi_i-\phi_j)]+V_{mj}^{2/3}[-1+\mu_j(1-2x_i)(\phi_j-\phi_i)]}{x_iV_{mi}^{2/3}[1+\mu_ix_j(\phi_i-\phi_j)]+x_jV_{mj}^{2/3}[1+\mu_jx_i(\phi_j-\phi_i)]}\right]\right] \quad (16)$$

The heat of formation ΔH_{AB} for a liquid solution or a solid solution is derived from Equation (17):

$$\Delta H_{AB} = f_{AB}\frac{x_i[1+\mu_ix_j(\phi_i-\phi_j)]x_j[1+\mu_jx_i(\phi_j-\phi_i)]}{x_iV_{mi}^{2/3}[1+\mu_ix_j(\phi_i-\phi_j)]+x_jV_{mj}^{2/3}[1+\mu_jx_i(\phi_j-\phi_i)]} \quad (17)$$

Then, if a binary alloy is a transition metal–transition metal alloy or a non-transition metal with a non-transition metal alloy, f_{AB} is defined by Equation (18). However, when a binary alloy is composed of a transition metal and a non-transition metal, the d-electrons of the transition metal and the p-electrons of the non-transition metal come into contact, leading them to hybridize with each other and lowering the energy, so the f_{AB} is calculated according to Equation (19).

$$f_{AB} = \frac{2PV_{mi}^{2/3}V_{mj}^{2/3}\{q/P[(\,n_{ws}^{1/3})_i-(n_{ws}^{1/3})_j]^2-(\phi_i-\phi_j)^2\}}{(n_{ws}^{1/3})_i^{-1}+(n_{ws}^{1/3})_j^{-1}} \quad (18)$$

$$f_{AB} = \frac{2PV_{mi}^{2/3}V_{mj}^{2/3}\{q/P[(\,n_{ws}^{1/3})_i-(n_{ws}^{1/3})_j]^2-(\phi_i-\phi_j)^2-\alpha(r/P)_i(r/P)_j\}}{(n_{ws}^{1/3})_i^{-1}+(n_{ws}^{1/3})_j^{-1}} \quad (19)$$

where ϕ_i and n_{wsi} are the electronegativity and electron density of element i, respectively; μ, r/P and α are the empirical constants and diverse metals have different values, which are listed in Table 2, specifically noting the constants α in liquid and solid alloys have corresponding values of 0.73 and 1; q/P is a constant with the value of 9.4; P is also a constant and the value varies depending on the alloy property, which is 14.20, 12.35, and 10.70 for a transition metal with a transition metal alloy, a transition metal with a non-transition metal alloy, and a non-transition metal with a non-transition metal alloy, respectively; and α_{ij} is defined as $\alpha_{ij}=1-1/14T(1/T_{mi}+1/T_{mj})$.

Table 2. The corresponding parameters of the Miedema model [30]. Reprinted from Ref. [30].

i	Property	ϕ	$n_{ws}^{1/3}$	μ	r/P
Ag	Transition metal	4.45	1.39	0.07	0.15
Cu	Transition metal	4.55	1.47	0.07	0.3
Sb	Non-transition metal	4.40	1.26	0.04	2.3

2.1.3. RSM and SRSM

The RSE [31] focuses on the role of excess molar enthalpy, which assumes the excess molar volume and excess molar entropy are both zero, so the excess molar Gibbs free energy is equal to the excess molar enthalpy and the expression is shown as follows:

$$\Delta G_m^E = \Delta H_m = \alpha x_i x_j \quad (20)$$

Then, according to the relationship $(\partial G_M^E/\partial x_i)_{T,P,i\neq j} = RT\ln\gamma_i$, the activity coefficients of i and j are:

$$\ln \gamma_i = \alpha x_i^2/RT, \; \ln \gamma_j = \alpha x_j^2/RT \quad (21)$$

where α is dependent on the temperature and can be attained according to Equation (22), while $\ln \gamma_i^\infty$ is the logarithm of the infinite activity coefficient.

$$\alpha = \frac{1}{2}\left(\alpha' + \alpha''\right) = \frac{RT}{2}\left(\ln \gamma_i^\infty + \ln \gamma_j^\infty\right) \tag{22}$$

Hardy [32] modified α based on the RSE and proposed the SRSE, which has a strong fitting effect for binary alloys, but it is not applicable for a multi-component system. The activity coefficient expression in a binary system is written as:

$$RT\ln \gamma_i = 2\alpha_{ij}\left(x_j^2 - x_j^3\right) + \alpha_{ji}(2\,x_j^3 - x_j^2) \tag{23}$$

where α_{ji} and α_{ij} are related to the temperature and calculated according to Equation (24).

$$\alpha_{ji} = RT \ln \gamma_i^\infty, \alpha_{ij} = RT \ln \gamma_j^\infty \tag{24}$$

2.2. Vacuum-Related Theoretical Knowledge

2.2.1. Separation Coefficient

The separation coefficient β plays a thoroughly significant role in research on the separation feasibility of an alloy by vacuum technology and is defined as follows:

$$\beta = \frac{\gamma_i}{\gamma_j} \cdot \frac{P_i^*}{P_j^*} \tag{25}$$

where γ_i and P_i^* are the activity coefficient and saturated vapor at a given temperature, respectively. P_i^* is obtained according to the Van Laar equation [33]:

$$\lg P_i^* = AT^{-1} + B\lg T + CT + D \tag{26}$$

where A, B, C and D are evaporation constants and are listed in Table 3 for Ag, Cu and Sb metals; T is the absolute temperature in Kelvin.

Table 3. The constants needed for calculation of the saturated vapor pressure [34]. Reprinted from Ref. [34].

i	A	B	C	D	Temperature Range, K
Ag	−14,400.00	−0.85	0.00	11.70	1234–2420
Cu	−17,520.00	−1.21	0.00	13.21	1356–2843
Sb	−6500.00	0.00	0.00	6.37	904–1948

2.2.2. Vapor–Liquid Equilibrium (VLE)

When using vacuum technology to separate alloys, VLE phase diagrams can exactly and quantitatively analyze the distribution of alloy components in the gas and liquid phases, which are classified into T–x–y and P–x–y diagrams. The important equations for obtaining the data of the VLE phase diagram are as follows:

$$y_i = \gamma_i x_i P_i^* / P \tag{27}$$

$$P = P_i^* \gamma_i x_i + P_j^* \gamma_j x_j \tag{28}$$

where x_i and y_i are separately the content of component i in the liquid and gas phases, as well as $x_i + x_j = 1$, $y_i + y_j = 1$; and P is the total system pressure (Ref. [35] describes this specific calculation process in detail).

Moreover, the vapor–liquid equilibrium phase composition is also a significant parameter to conduct the separation of alloys. For binary alloys, the vapor–liquid equilibrium phase composition can be calculated by Equation (29).

$$x_{i,\,g} = \left[1 + \frac{x_{j,\,l}}{x_{i,\,l}} \frac{\gamma_j}{\gamma_i} \frac{P_j^*}{P_i^*}\right]^{-1} \tag{29}$$

3. Analysis of Activity and Vacuum Foundation Separation

3.1. The Calculation and Testing of Predicted Activity

3.1.1. The Calculation of Predicted Activity and Comparison with Experimental Values

The degree to which the predicted activity and activity coefficient values of the MIVM, M-MIVM, Wilson equation, RSE, SRSE and Miedema model are in agreement with the experimental data in the Cu–Ag binary alloy at 1400 K and 1423 K, respectively, is shown in Figure 1(a_1–a_4). It is found that the Cu–Ag binary alloy is a symmetrical system (the curves of the experimental activity for two components converge at about $x = 0.5$ on the coordinate axis and are symmetrical at $x = 0.5$ or nearby). And it is remarkable that there is a larger disparity between the predicted values of the Miedema model and the experimental values, while these predicted values of the group elements Ag and Cu calculated from the other models apparently agree with the experimental values. Meanwhile, the predicted values of the Wilson equation and M-MIVM deviate a little from the experimental values of the Ag and Cu contents in the 0–0.2 range at 1400 K.
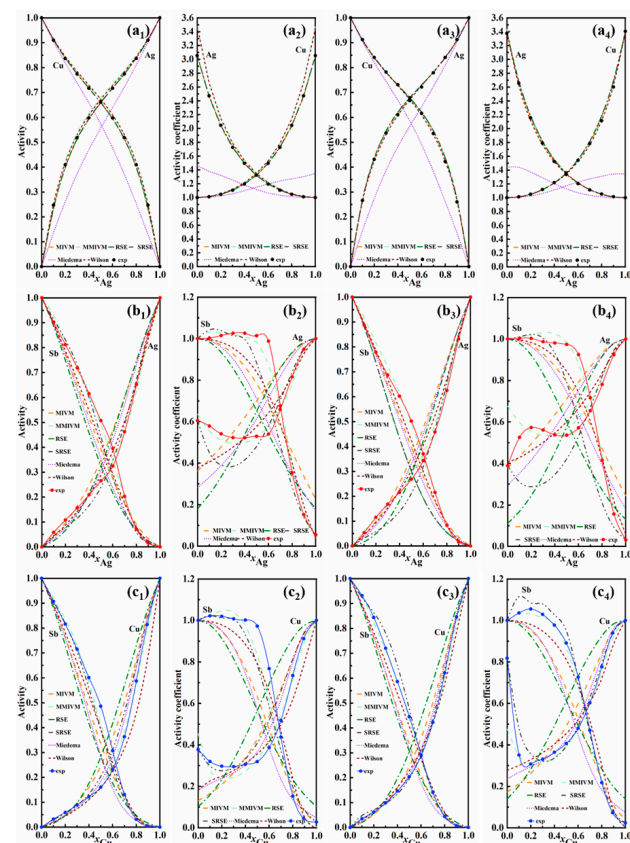

Figure 1. The comparison of the experimental values and prediction values calculated from six models for binary alloys in the Ag–Cu–Sb system at diverse temperatures: (a_1,a_2) activity and activity coefficient (Cu–Ag binary alloy at 1400 K); (a_3,a_4) activity and activity coefficient (Cu–Ag binary alloy at 1423 K); (b_1,b_2) activity and activity coefficient (Sb–Ag binary alloy at 1250 K); (b_3,b_4) activity and activity coefficient (Sb–Ag binary alloy at 1300 K); (c_1,c_2) activity and activity coefficient (Sb–Cu binary alloy at 1190 K); and (c_3,c_4) activity and activity coefficient (Sb–Cu binary alloy at 1375 K).

Figure 1(b$_1$–b$_4$) are the curves of the experimental values, the predicted activity and the activity coefficient values relating to the Ag component under 1250 K and 1300 K, respectively, showing that the Sb–Ag binary alloy is an asymmetric system. As shown in the plots, the trends of the activity coefficient and activity are much more sophisticated and it is observed that the MIVM, Wilson equation, RSE, SRSE and Miedema model are incapable, while the M-MIVM displays a relatively greater prediction capability for the alloy. In the meantime, when the Ag or Sb content is in the 0.6–1 range, the predicted activity values using the SRSE are likewise in agreement with the experimental values.

Functions of the activity and activity coefficient concerning with the Cu component at 1190 K and 1375 K, respectively, as displayed in Figure 1(c$_1$–c$_4$), show that the Sb–Cu binary alloy is an asymmetric system. The predicted values of the MIVM, Wilson equation, Miedema model, RSE and SRSE visibly disagree with the experimental values, except the M-MIVM. In addition, it is found that the SRSE model has great fitting ability for the Cu content in the range of 0.3–1 at 1375 K.

By preliminary judgment, among the binary alloys of the Ag–Cu–Sb system, the M-MIVM has the most ideal predictive performance and the SRSE also has good fitting ability but in a range of components, while the predictive ability of the Miedema model is relatively poor. In an attempt to accurately characterize the degree of error between the experimental values and predicted values, the average relative deviations S_i and the average standard deviations S_i^* of the six models are also calculated according to Equation (30) and are shown in Figure 2 and Table 4.

$$S_i = \pm \frac{100}{n} \sum_{i=1}^{n} \left| \frac{a_{i,\,pre.} - a_{i,\,exp.}}{a_{i,\,exp.}} \right|,\, S_i^* = \pm \left[\frac{1}{n} \sum_{i=1}^{n} \left(a_{i,\,pre.} - a_{i,\,exp.} \right)^2 \right]^{1/2} \tag{30}$$
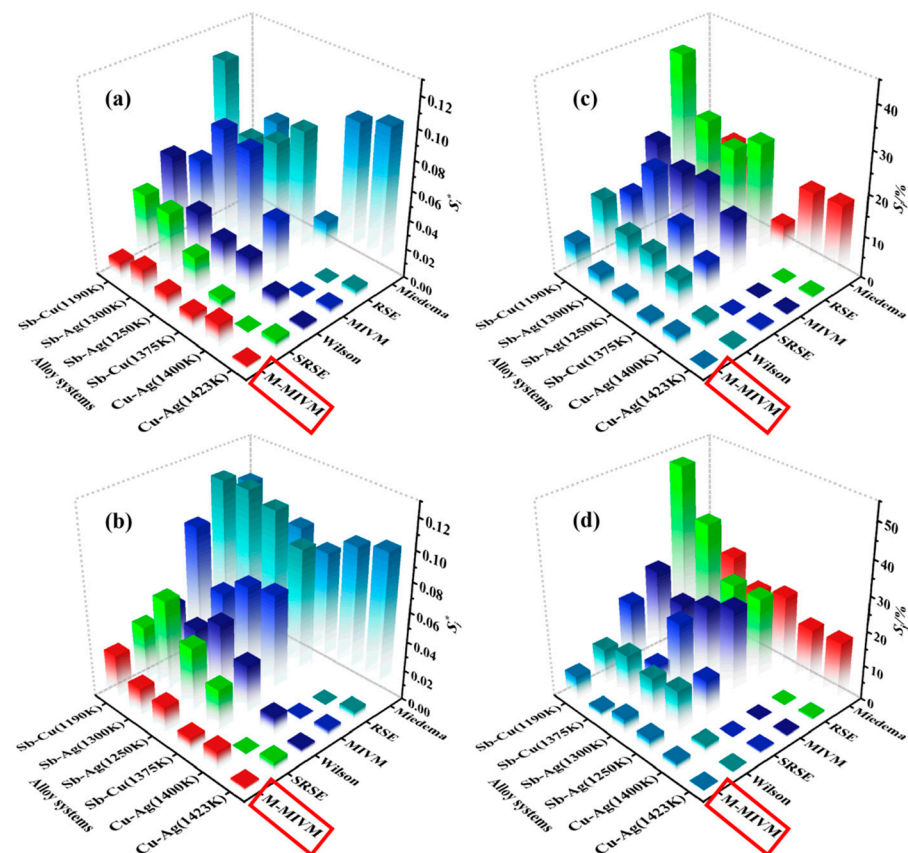
Figure 2. The deviation of each model in binary alloys of the Ag–Cu–Sb system: (**a**) the average standard deviation S_i^*; (**b**) the average standard deviation S_j^*; (**c**) the average relative deviation S_i; and (**d**) the average relative deviation S_j.

Table 4. The average relative deviation S and average standard deviation S^* of the MIVM, M-MIVM, Wilson equation, Miedema model, RSE and SRSE.

Model and Parameter ($\pm$)	System i–j	Cu–Ag	Cu–Ag	Sb–Ag	Sb–Ag	Sb–Cu	Sb–Cu	Overall Mean ($\bar{S}_2^*$ and $\bar{S}_2$/%)
Temperature/K		1400	1423	1250	1300	1190	1375	—
MIVM	S_i^*	0.00183	0.00557	0.08109	0.08616	0.05588	0.04337	0.04811
	S_j^*	0.00185	0.00546	0.07082	0.05723	0.09332	0.07473	
	S_i/%	0.29677	0.67817	20.84227	20.06200	23.88805	15.58372	15.21472
	S_j/%	0.29570	0.93796	27.71771	24.22359	26.93817	21.11248	
M-MIVM	S_i^*	0.01777	0.00304	0.01396	0.01932	0.01335	0.01156	0.01501
	S_j^*	0.01375	0.00295	0.01981	0.02119	0.03307	0.01038	
	S_i/%	3.37258	0.38438	3.77585	5.48706	9.23449	2.62595	3.97278
	S_j/%	2.69677	0.51095	4.22243	5.01305	7.88977	2.46013	
Wilson equation	S_i^*	0.01332	0.00424	0.02886	0.03808	0.06750	0.02807	0.03171
	S_j^*	0.01358	0.00415	0.05475	0.04193	0.04837	0.03770	
	S_i/%	2.61367	0.69341	10.83764	11.55478	16.32505	8.37948	8.71565
	S_j/%	2.64407	0.57929	13.15704	12.06339	11.58937	14.15068	
Miedema model	S_i^*	0.09956	0.10500	0.06127	0.07419	0.03573	0.02209	0.07970
	S_j^*	0.09754	0.10278	0.09335	0.07176	0.10818	0.08499	
	S_i/%	18.38577	18.80675	19.16126	20.75625	14.49344	6.92024	19.92938
	S_j/%	17.99045	18.39257	23.41028	21.11154	32.23751	27.48654	
RSE	S_i^*	0.00028	0.00691	0.07727	0.07100	0.11520	0.09337	0.06783
	S_j^*	0.00028	0.00702	0.11246	0.11789	0.11666	0.09560	
	S_i/%	0.03924	1.01096	25.28264	28.82336	41.28900	29.47973	22.83921
	S_j/%	0.03924	1.14580	26.73625	26.73810	53.07023	40.41595	
SRSE	S_i^*	0.00028	0.00726	0.02815	0.04816	0.05041	0.01054	0.02891
	S_j^*	0.00028	0.00713	0.04922	0.07043	0.04300	0.03205	
	S_i/%	0.03924	1.02258	13.74654	23.41977	14.24080	8.35729	10.43569
	S_j/%	0.03924	1.20000	11.68295	23.56618	21.22542	6.68830	

Figure 2 shows that the values of the S_i, S_j, S_i^* and S_j^* of the M-MIVM are the smallest among the six models, which indicates that the M-MIVM has the higher reliability, adaptability and universality and means that the data of binary alloys in the Ag–Cu–Sb system from the M-MIVM can be applied in the prediction of the activity or activity coefficient of the Ag–Cu–Sb ternary alloy.

The $\bar{S}_2$ (the overall mean value of S_i and S_j for all the binary alloys of the Ag–Cu–Sb system, which comprises all temperatures) and $\bar{S}_2^*$ (the overall mean value of S_i^* and S_j^* for all the binary alloys of the Ag–Cu–Sb system, which comprises all temperatures) of the M-MIVM are 0.01501 and 3.97278%, respectively, which are about two to six times less than those of the other five models ($\bar{S}_{2\mathrm{Mie}}^* = 0.07970 > \bar{S}_{2\mathrm{RS}}^* = 0.06783 > \bar{S}_{2\mathrm{MI}}^* = 0.04811 > \bar{S}_{2\mathrm{Wil}}^* = 0.03171 > \bar{S}_{2\mathrm{SR}}^* = 0.028$, $\bar{S}_{2\mathrm{RS}} = 22.83921\% > \bar{S}_{2\mathrm{Mie}} = 19.92938\% > \bar{S}_{2\mathrm{MI}} = 15.21472\% > \bar{S}_{2\mathrm{SR}} = 10.43569\% > \bar{S}_{2\mathrm{Wil}} = 8.71565\%$), as Table 4 reveals. This means that the prediction capacity and effect of the M-MIVM are better than the other models for the system; in other words, it indicates the stability and reliability of the M-MIVM. Thus, the M-MIVM, with excellent data fitting capability, can accurately describe the characteristics of these alloys, which in turn enhances the calculation precision of the separation coefficient, VLE and evaporation rate data in vacuum separation. Meanwhile, for the M-MIVM, the S_e (($S_i + S_j$)/2) and $\bar{S}_e^*$(($\bar{S}_i^* + \bar{S}_j^*$)/2) of the Cu–Ag binary alloy at 1423 K are the lower than those at 1400 K. Similarly, the S_e and $\bar{S}_e^*$ of the Sb–Ag binary alloy at 1250 K and the Sb–Cu binary alloy at 1375 K are superior to those of the Sb–Ag binary alloy at 1300 K and the Sb–Cu binary alloy at 1190 K, respectively. What has been mentioned above means that the predicted values of the Cu–Ag binary alloy at 1423 K, Sb–Ag binary alloy at 1250 K and Sb–Cu binary alloy at 1375 K in the M-MIVM are optimal for further activity prediction of the Ag–Cu–Sb

ternary alloy and vacuum separation foundational research on the Cu–Ag, Sb–Ag and Sb–Cu binary alloys.

As illustrated in Table 4, the S_i, S_j, S_i^* and S_j^* of each model in the Sb–Ag and Sb–Cu binary alloys are much larger than those of the Cu–Ag binary alloy, again indicating that they are asymmetric systems. Because of the strong molecular interaction between Ag, Ag_3Sb, $Ag_{17}Sb_3$ and Sb in the Sb–Ag binary alloy (Cu, Cu_3Sb, Cu_2Sb and Sb in the Sb–Cu binary alloy), the activity of the Sb–Ag binary alloy (Sb–Cu binary alloy) deviates from the ideal solution by a large margin, which cannot be depicted by the RSE, SRSE, Wilson equation and MIVM. The RSE and SRSE pay more attention to the contribution of excess entropy to the excess Gibbs free energy, ignoring the role of excess enthalpy, and the Wilson equation emphasizes the contribution of excess enthalpy to the excess Gibbs free energy. Although the MIVM expresses both the excess enthalpy and the excess entropy, which can simultaneously describe the change in volume (entropy) and strong molecular interaction (enthalpy) caused by the mixing of heterogeneous molecules, the connectivity between the enthalpy and entropy parameters is too close together, which limits the fitting capability of the MIVM. Thus, the M-MIVM separates the enthalpy and entropy parameters based on the radial distribution theory, which can freely switch the predominant role of enthalpy or entropy. In the meantime, the complexity of the enthalpy expression is increased by drawing on the Scatchard–Hildebrand theory. These improvements not only maintain the excellent forecasting capability of the MIVM, Wilson equation, RSE and SRSE for a symmetric system but also boast good predictive ability for asymmetric systems. This study may provide supplementary evidence that the M-MIVM unquestionably makes up for the drawbacks of other conventional models in asymmetric systems. Thus, the M-MIVM is a comprehensive optimal model for the activity prediction of the Ag–Cu–Sb system.

3.1.2. Testing Activity Data by Herington Test

Accurate predictive activity data can not only solve the problems of inaccurate activity data under high-temperature experimental conditions, which is time-consuming and labor-intensive in the measurement process, but can also be directly applied to quantitative thermodynamic calculations and analyses in the following vacuum studies for the Ag–Cu, Ag–Sb and Cu–Sb binary alloys in terms of the VLE and separation coefficient. Herington and many scholars [36] always check the reliability of activity data by D in the chemical field, which was defined by Equation (31). And when $D < 3$, the activity data of this system are considered reliable.

$$D = 100 \left| \frac{S_A - S_B}{S_A + S_B} \right| = 100 \frac{\left| \int_0^1 \ln \gamma_1 / \gamma_2 \mathrm{d}x_1 \right|}{\int_0^1 |\ln \gamma_1 / \gamma_2| \mathrm{d}x_1} \tag{31}$$

So, this work checks the predictive activity calculated by the M-MIVM for the Cu–Ag binary alloy at 1423 K, Sb–Ag binary alloy at 1250 K and Sb–Cu binary alloy at 1375 K based on the thermodynamic consistency to enhance the reliability of the predictive activity data. As Figure 3a–c show, the distance between A and B is approximately equal, while the area residuals are $2.964\mathrm{E}^{-3}$, 0.75589 and 1.92475, separately, which are all less than 3. This result shows that the activity data calculated by the M-MIVM meet the needs of testing the thermodynamic consistency and are credible for the Cu–Ag, Sb–Ag and Sb–Cu binary alloys.
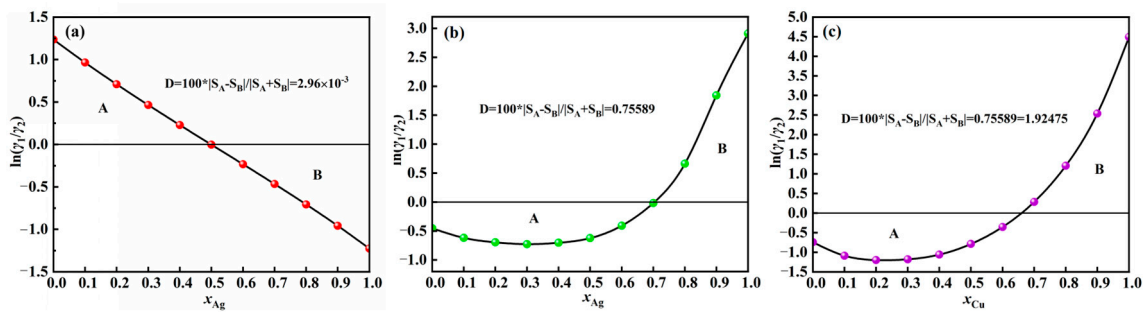
Figure 3. Testing the thermodynamic consistency of the activity coefficient calculated by the M-MIVM for binary alloys in the Ag–Cu–Sb system at different temperatures: (**a**) Cu–Ag binary alloy at 1423 K; (**b**) Sb–Ag binary alloy at 1250 K; and (**c**) Sb–Cu binary alloy at 1375 K.

3.2. Vacuum Separation Foundational Research Based on M-MIVM

3.2.1. Separation Coefficient

The separation coefficients of the Sb–Ag and Sb–Cu binary alloys are both much smaller than one, being in the order of magnitude 10^{-4}~10^{-2} and 10^{-6}~10^{-2}, respectively, according to Figure 4. This indicates that these alloys may be easily separated by vacuum technology and that the Sb will be taken to the vapor phase. The separation coefficient of the Cu–Ag binary alloy is 200~8 in the temperature scope of 1473~1873 K, which means that this alloy is adversely separated by the method (a separation coefficient much larger than 1 or much smaller than 1 favors separation of the alloy, while equal to 1 or closer to 1 is detrimental to separation of the alloy). In addition, the separation coefficients of the binary alloys of the Ag–Cu–Sb system are closer to the value of 1 with the temperature increasing, implying that the relatively low temperature is conducive to the separation of these alloys and when the component *i* of any binary alloy rises in the range from 0 to 1, the alloy is harder to separate by this approach.
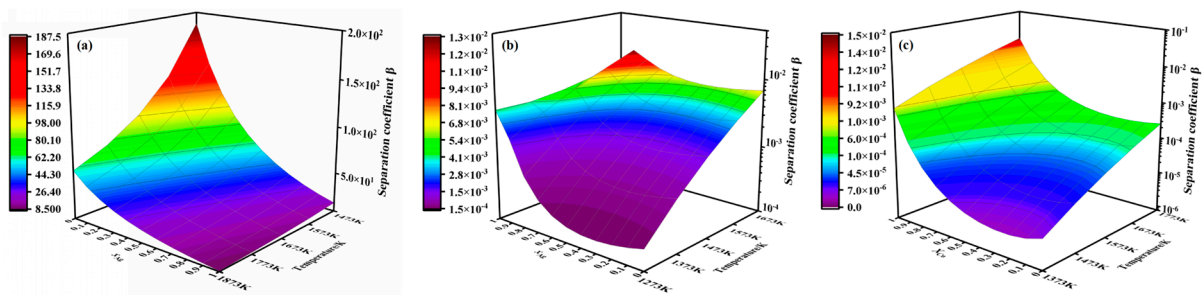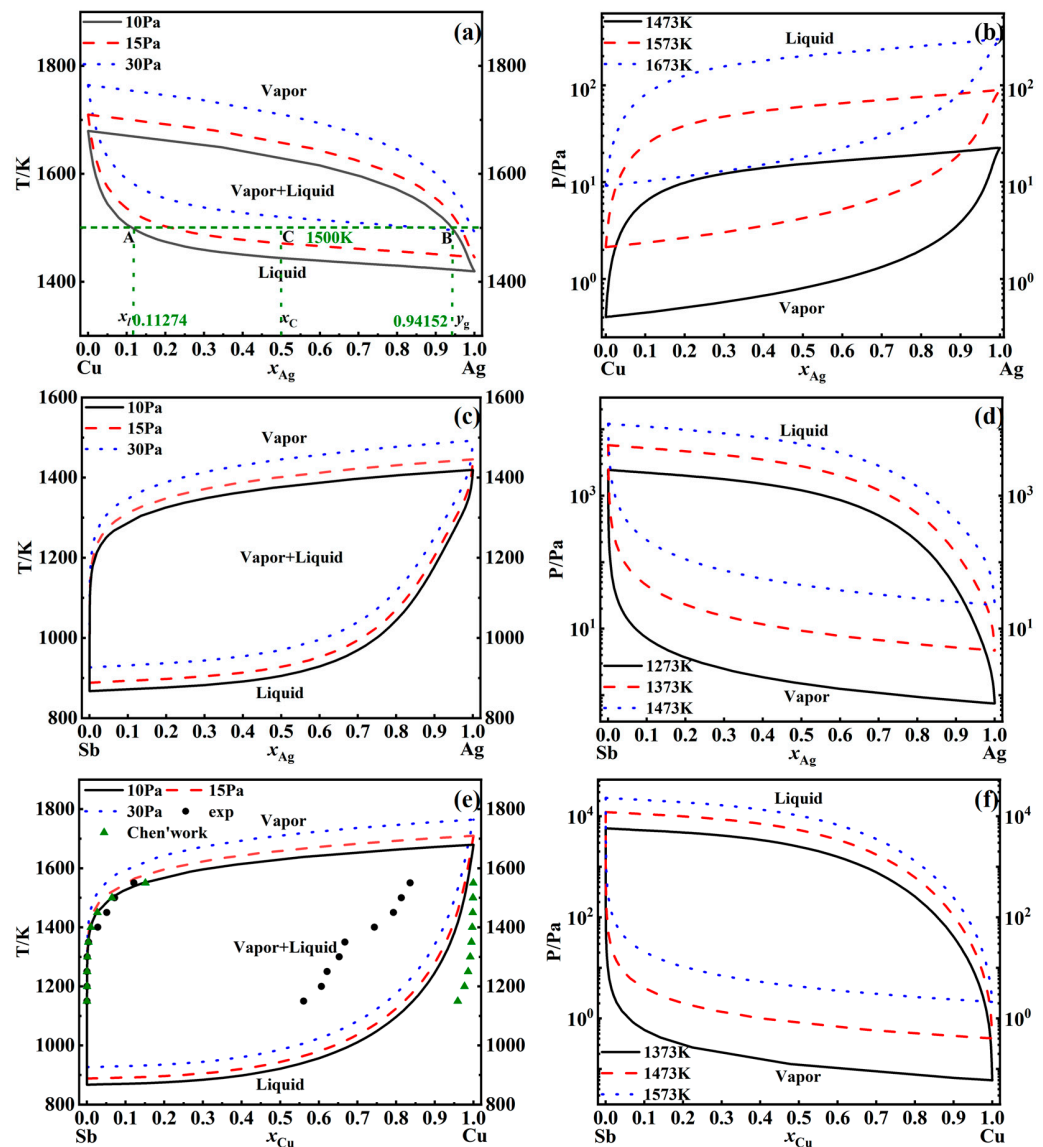

Figure 4. Separation coefficient *β* for binary alloys in the Ag–Cu–Sb system at diverse temperatures: (**a**) Cu–Ag binary alloy (1473~1873 K); (**b**) Sb–Ag binary alloy (1273~1673 K); and (**c**) Sb–Cu binary alloy (1373~1773 K).

3.2.2. VLE

The temperatures of the vapor phase line, the liquid phase line and the range between these two lines decrease as the pressure decreases, indicating that low pressure is conducive to lowering the separation temperature of the Cu–Ag binary alloy (Sb–Ag binary alloy or Sb–Cu binary alloy), as shown in Figure 5a,c,e. They are *T*–*x*–*y* diagrams of binary alloys in the Ag–Cu–Sb system at diverse pressures. In addition, the optimal separation temperature can be inferred according to the *T*–*x*–*y* diagram. For instance, under the condition of 10 Pa, a Cu–Ag binary alloy could achieve a silver content of greater than 0.9999 in the gas phase at a temperature of 1419.00 K, and it may yield a copper content of greater than 0.9999 in the liquid phase at a temperature of 1649.00 K. What is more, if the temperature and pressure are determined, the masses of the distillate and residue can be qualitatively predicted using the *T*–*x*–*y* diagram. Taking the Cu–Ag binary alloy as an illustration, under the condition of 1500 K and 10 Pa, a Cu–Ag binary alloy with 100 g containing a 50% silver content

should theoretically yield a distillate containing 46.73 g and a 53.27 g of residue using the leverage theorem.

Figure 5. The VLE phase diagram of binary alloys in the Ag–Cu–Sb system at diverse temperatures or pressures: (**a**) *T*–*x*–*y* of the Cu–Ag binary alloy (10~30 Pa); (**b**) *P*–*x*–*y* of the Cu–Ag binary alloy (1473~1673 K); (**c**) *T*–*x*–*y* of the Sb–Ag binary alloy (10~30 Pa); (**d**) *P*–*x*–*y* of the Sb–Ag binary alloy (1273~1473 K); (**e**) *T*–*x*–*y* of the Sb–Cu binary alloy (10~30 Pa); and (**f**) *P*–*x*–*y* of Sb–Cu binary alloy (1373~1573 K).

From Figure 5b,e,f, another type of VLE diagram, it can be seen that a low separation temperature requires a low pressure. Under the same temperature condition, the silver content of the Cu–Ag binary alloy in the vapor phase is positively correlated with the pressure, while the silver content of the Sb–Ag binary alloy in the vapor phase and the copper content of the Sb–Cu binary alloy in the vapor phase are both negatively bound up with the pressure. In the meantime, with the pressure increasing, the copper content of the Cu–Ag binary alloy in the liquid phase drops but the antimony content of the Sb–Ag binary alloy (Sb–Cu binary alloy) in the liquid phase increases. In *P*–*x*–*y* diagrams, we can also gain the theoretical conclusions like in the *T*–*x*–*y* diagram of the Cu–Ag binary alloy, which could guide vacuum separation experiments and industrial production.

This work focuses on the Ag–Cu binary alloy due to the conclusion of the separation coefficient. According to Equation (29), the VLE phase compositions of the Ag–Cu alloy at diverse temperatures are displayed in Figure 6. It can be seen that higher temperatures are less favorable for Ag–Cu alloy separation and that a higher copper content is also detrimental to the separation of the Ag–Cu alloy. For instance, when the content of Ag in the liquid phase is 70%, there is 98% Ag in the gas phase at 1473 K but less than 96% Ag in the gas phase at 1873 K. And at the same temperature, 1873 K, the Ag–Cu alloy containing 90% copper has 6% less silver in the gas phase than the Ag–Cu alloy containing 80% copper, indicating it is difficult to obtain high-purity sliver in the gas phase by vacuum technology in an Ag–Cu alloy of low-grade silver.
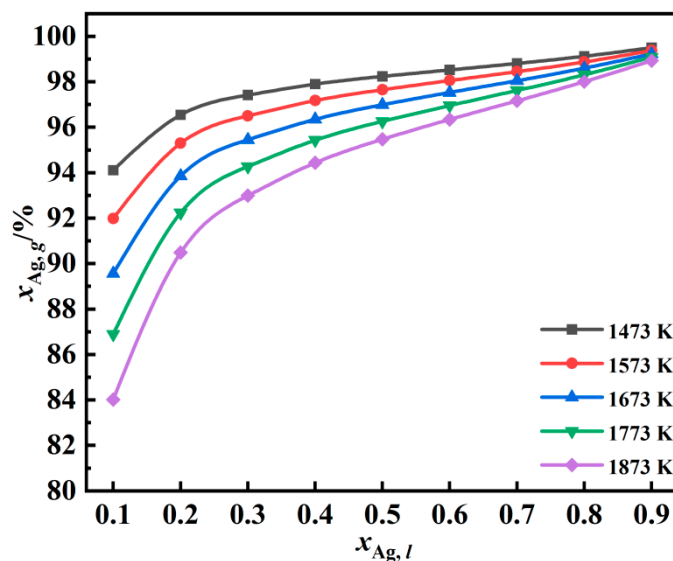

Figure 6. The VLE phase composition of the Ag–Cu alloy at diverse temperatures.

3.2.3. Testing VLE Data by Existing Experimental Values

As mentioned before, the VLE data were important in guiding the experimental process and production practices of alloy separation, so this work also conducted the validation of the theoretical VLE data using the available experimental values.

Van Ness [37] proposed a point test that can directly examine the experimental VLE data, as shown in Equation (32). When $y_{(MAD)}$ < 1, the experiment VLE data of this system were thought to be dependable.

$$y_{(MAD)} = \frac{1}{N}\sum_{i=1}^{N} 100\left|y_i^{exp} - y_i^{cal}\right| \tag{32}$$

Thus, this method is also followed in this work to test the theoretical VLE data and simultaneously perform a comparison of the experimental and theoretical values by Δy. According to Tables 5 and 6, it can be seen that the deviation of the vapor phase composition is very small, indicating that the M-MIVM is reliable in predicting the VLE results of the Ag–Cu and Cu–Sb binary alloys. In addition, the $y_{(MAD)}$ in the Cu–Sb binary alloy is <1, but that of the Ag–Cu binary alloy is >1, meaning the experimental VLE data of this alloy are undependable. The main reasons for the deviation are: (1) the M-MIVM is calculated on the basis of ideal conditions, while the experimental conditions of high temperature and low pressure for the alloy separation cannot reach the ideal equilibrium state, in addition the mass losses or the metal vapor cannot return to the liquid phase after condensation can cause errors; and (2) there are errors in the chemical analysis of the experimental results. Otherwise, with the same liquid composition with 4.68% sliver in the liquid phase under the condition of 1573 K, there is 76.434% (mole fraction) sliver in the gas phase by

experiment [38] and 78.452% sliver in the gas phase by theoretical calculation, meaning the experimental result deviates very little from the theoretical consequence.

Table 5. Vapor–liquid equilibrium calculation results, experimental conditions and experimental results [38] in the Ag–Cu alloy. Reprinted from Ref. [38].

| No	T/K	P/Pa	$x_{Ag,exp}$	$y_{Ag,exp}$	$y_{Ag,cal}$	Δy_{max} [a]	$y_{(MAD)}$
1	1573	15~30	0.57446	0.91944	0.98247~0.98479	0.06534	
2	1673	15~30	0.51283	0.92193	0.98016~0.98287	0.06095	
3	1773	15~30	0.45776	0.90619	0.97794~0.98097	0.07479	4.75846~4.97882
4	1873	15~30	0.26084	0.93835	0.96451~0.98479	0.03130	
5	1973	15~30	0.00613	0.35774	0.33898~0.37431	0.01657	

[a] $\Delta y_{max} = \text{Max} \, |y_{i,exp} - y_{i,cal}|$.

Table 6. Vapor–liquid equilibrium calculation results, experimental conditions and experimental results [39] in the Cu–Sb alloy. Reprinted from Ref. [39].

No	T/K	P/Pa	$x_{Cu,exp}$	$y_{Sb,exp}$	$y_{Sb,cal}$	Δy [a]	$y_{(MAD)}$
1	1150	10	0.60660	0.99990	$9.9999999384 \times 10^{-1}$	9.99938×10^{-5}	
2	1200	10	0.62130	0.99980	$9.9999999110 \times 10^{-1}$	0.00020	
3	1250	10	0.65250	0.99960	$9.9999997968 \times 10^{-1}$	0.00040	0.66400
4	1300	10	0.66710	0.99560	$9.9999996942 \times 10^{-1}$	0.00440	
5	1350	10	0.74360	0.97190	$9.9999966354 \times 10^{-1}$	0.02810	

[a] $\Delta y = |y_{i,exp} - y_{i,cal}|$.

Moreover, as demonstrated in Figure 7, the amount of silver in the gas phase decreases from 79.04% to 33.24% as the temperature increases from 1573 K to 1973 K for the $1x_l$% Ag–Cu binary alloy, while the amount of silver in the gas phase decreases from 100% to 85.17% as the temperature increases 1573~1873 K for the $58x_l$% Ag–Cu binary alloy, and the higher the Cu content in the liquid and the lower the silver content in the gas phase. These experimental results are consistent with the theoretical calculations and prove the appearance of VLE phase composition in the Ag–Cu alloy.
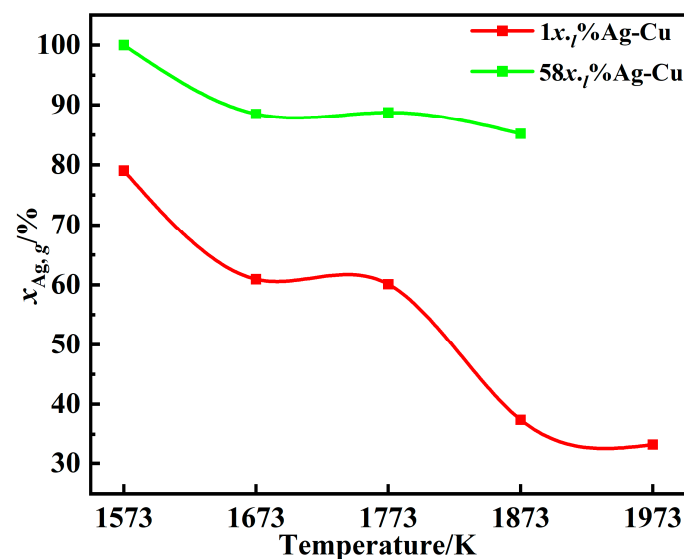
Figure 7. The vapor–liquid phase composition of the Ag–Cu alloy at diverse temperatures in experiments [38]. Adapted from Ref. [38].

So, this work's VLE results based on the M-MIVM are reliable and reaffirm that the M-MIVM is dependable.

4. Conclusions

(1) The results of the deviations for the M-MIVM are the smallest, with an overall mean of the average standard deviation of 0.01501 and the average relative deviation of 3.97278%. In addition, the predicted values of the Cu–Ag binary alloy at 1423 K, Sb–Ag alloy at 1250 K and Sb–Cu alloy at 1375 K calculated from the M-MIVM are more reliable and pass the thermodynamic consistency test.

(2) On the basis of the M-MIVM, this work launches the vacuum separation theoretical research on the Cu–Ag, Sb–Ag and Sb–Cu binary alloys. The Cu–Ag binary alloy is relatively harder to separate than other alloys, with the value of separation coefficient of 200~8 in the temperature scope from 1473 K to 1873 K.

(3) The precise experimental conditions for the separation of the Cu–Ag, Sb–Ag and Sb–Cu binary alloys may be able to be determined according to the VLE. At 10 Pa and 1419 K, a Cu–Ag alloy could theoretically achieve a silver content of greater than 0.9999 in the gas phase. And there is 78.452% sliver in the gas phase by theoretical calculation with 0.0468 sliver in the liquid phase for the Ag–Cu binary alloy at 1573 K, which is in general agreement with the experiment.

(4) The M-MIVM is the optimal model for further predicting the activity of the Ag–Cu–Sb ternary alloy, according to above activity conclusion, combining analysis of the derivation process of the excess Gibbs free energy and a comparison between the theoretical values and experimental data in the VLE.

(5) These results mentioned above can guide research on the activity of the Ag–Cu–Sb ternary alloy and its subsystems in vacuum separation experiments and industrial production. The activity of the Ag–Cu–Sb ternary alloy will be investigated based on the parameters of its binary alloys calculated from the M-MIVM.

Author Contributions: Investigation, Q.L. and Y.T.; data curation, Q.L.; writing—original draft preparation, Q.L.; methodology, Y.T. and B.Y.; resources, Y.T., L.W. and W.J.; supervision, B.Y., B.X. and W.J.; writing—review and editing, Q.L., Y.T., L.K. and L.W.; software: L.K. and B.X.; formal analysis, B.Y. and B.X.; funding acquisition: W.J.; validation: L.K. and L.W. All authors have read and agreed to the published version of the manuscript.

Data Availability Statement: The original contributions presented in the study are included in the article, further inquiries can be directed to the corresponding author.

Conflicts of Interest: The authors declare no conflict of interest.

References

1. Zhang, C.Q.; Li, S.Z.; Liu, L.H.; Feng, X.D.; Liu, G. Silver-catalyzed and silver-promoted reactions of isocyanides. *Eur. J. Org. Chem.* **2023**, *26*, e202300323. [CrossRef]
2. Rautio, T.; Torbati-Sarraf, H.; Allam, T.; Järvenpää, A.; Hamada, A. Enhancement of electrical conductivity and corrosion resistance by gold-nickel coating of additively manufactured AlSi10Mg alloy. *J. Mater. Res. Technol.* **2022**, *17*, 521–536. [CrossRef]
3. Quintana, C.; Cifuentes, M.P.; Humphrey, M.G. Transition metal complex/gold nanoparticle hybrid materials. *Chem. Soc. Rev.* **2020**, *49*, 2316–2341. [CrossRef] [PubMed]
4. Zhan, H.J.; Guo, J.Y.; Shen, J.L.; Wang, X.R.; Fan, Z.H.; Guo, B.; Liu, W. Synthesis of Silver Flakes and Their Application as Conductive Filler for Low-Curing-Temperature Silver Pastes. *J. Electron. Mater.* **2019**, *48*, 2745–2753. [CrossRef]
5. Dong, Z.L.; Jiang, T.; Xu, B.; Yang, J.K.; Chen, Y.Z.; Li, Q.; Yang, Y.B. Comprehensive recoveries of selenium, copper, gold, silver and lead from a copper anode slime with a clean and economical hydrometallurgical process. *Chem. Eng. J.* **2020**, *393*, 124762. [CrossRef]
6. Xu, B.; Yang, Y.B.; Li, Q.; Yin, W.; Jiang, T.; Li, G.H. Thiosulfate leaching of Au, Ag and Pd from a high Sn, Pb and Sb bearing decopperized anode slime. *Hydrometallurgy* **2016**, *164*, 278–287. [CrossRef]

7.   Xing, W.D.; Lee, M.S. Development of a hydrometallurgical process for the recovery of gold and silver powders from anode slime containing copper, nickel, tin, and zinc. *Gold Bull.* **2019**, *52*, 69–77. [CrossRef]

8.   Xiao, L.; Wang, Y.L.; Yu, Y.; Fu, G.Y.; Han, P.W.; Sun, Z.H.I.; Ye, S.F. An environmentally friendly process to selectively recover silver from copper anode slime. *J. Clean. Prod.* **2018**, *187*, 708–716. [CrossRef]

9.   You, Y.J.; Xu, J.J.; Kong, L.X.; Xu, B.Q.; Yang, B. Kinetics study of Pb evaporation from pure Pb and Pb-Ag alloy in vacuum evaporation process. *J. Mater. Res. Technol.* **2021**, *15*, 7012–7021. [CrossRef]

10.   Zhang, X.X.; Friedrich, S.; Friedrich, B. Separation behavior of arsenic and lead from antimony during vacuum distillation and zone refining. *J. Mater. Res. Technol.* **2020**, *9*, 4386–4398. [CrossRef]

11.   Khlebnikov, A.I. Modern industrial experience of application of vacuum distillation of silver for separation of gold-silver alloy. *Tsvetnye Metally.* **2014**, *7*, 25–28.

12.   Wang, S.P.; Zhao, J.Y.; Xu, B.Q.; Kong, L.X.; Jiang, W.L.; Yang, B. Theoretical research on vacuum separation of Au-Ag alloy. *Trans. Nonferrous Met. Soc. China* **2022**, *32*, 2719–2726. [CrossRef]

13.   Wang, S.P.; Chen, L.L.; Xu, B.Q.; Jiang, W.L.; Kong, L.X.; Yang, B.; Xiong, H.; Qu, C.; Zhang, T.; Zhang, S.H.; et al. Theoretical calculation and experimental investigation on vacuum gasification separation of Ag-Cu-Au ternary alloy. *J. Alloys Compd.* **2023**, *948*, 169685. [CrossRef]

14.   Yi, J.F.; Zha, G.Z.; Huang, D.X.; Kong, X.F.; Yang, B.; Liu, D.C.; Xu, B.Q. Effective separation and recovery of valuable metals from high value-added lead anode slime by sustainable vacuum distillation. *J. Clean. Prod.* **2021**, *319*, 128731. [CrossRef]

15.   Werner, J.; Seidel, T.; Jafar, R.; Heese, R.; Hasse, H.; Bortz, M. Multiplicities in thermodynamic activity coefficients. *AIChE J.* **2023**, e18251. [CrossRef]

16.   Jiao, J.M.; Ma, W.H.; Sun, Y.; Tao, D.P.; Huang, X.; Wu, J.J.; Dai, Y.N. Application of molecular interaction volume model for predicting the Ca activity coefficients in Si-Ca binary and Si-Ca-Pb ternary alloys. *Vacuum* **2016**, *128*, 106–111. [CrossRef]

17.   Hou, W.Y.; Wang, J.R.; Li, H.S. Theoretical Investigation of Thermodynamic Properties of the Al-Si-Fe Ternary Alloy. *ACS Omega* **2024**, *9*, 6316–6324. [CrossRef] [PubMed]

18.   Yao, S.; Duan, S.C.; Guo, H.J.; Guo, J. Thermodynamic Properties Prediction of Fe-Al-Ti Alloys Based on Atom and Molecule Coexistence Theory. *Phys. Met. Metallogr.* **2022**, *123*, 1287–1298. [CrossRef]

19.   Oshakuade, O.M.; Awe, O.E. Computation of infinite dilute activity coefficients for Ga-X (X= In, Tl) and thermodynamic activities of all components in liquid Ga-In-Ti alloys. *Phys. Chem. Liq.* **2022**, *60*, 427–435. [CrossRef]

20.   Prausnitz, J.M.; Lichtenthaler, R.N.; Azevedo, E.G.D. *Molecular Thermodynamics of Fluid-Phase Equilibria*; Prentice-Hall: Upper Saddle River, NJ, USA, 1986.

21.   Dadmohammadi, Y.; Gebreyohannes, S.; Neely, B.J.; Gasem, K.A.M. Application of Modified NRTL Models for Binary LLE Phase Characterization. *Ind. Eng. Chem. Res.* **2018**, *57*, 7282–7290. [CrossRef]

22.   Seyf, J.Y.; Shojaeian, A. Vapor-liquid (azeotropic systems) and liquid-liquid equilibrium calculations using UNIFAC and NRTL-SAC activity coefficient models. *Fluid Phase Equilibr.* **2019**, *494*, 33–44. [CrossRef]

23.   Xu, J.J.; Kong, L.X.; Xu, B.Q.; Ren, J.Q.; Li, Y.F.; Li, L.; Liu, D.C.; Yang, B. Vacuum separation of zinc-silver alloy: Measurement and modeling of vapor-liquid equilibrium. *Vacuum* **2021**, *189*, 110245. [CrossRef]

24.   Hultgren, R.; Desai, P.D.; Hawkins, D.T.; Gleiser, M.; Kelley, K.K. *Selected Values of the Thermodynamic Properties of Binary Alloys*; American Society for Metals: Detroit, MI, USA, 1973.

25.   SGTE; Equilibria, P. *Crystallographic and Termodynamic Data of Binary Alloys*; New Series IV/19B, Landolt-börnstein-Group IV Physical Chemistry; Springer: Berlin/Heidelberg, Germany, 2002.

26.   Tao, D.P. A new model of thermodynamics of liquid mixtures and its application to liquid alloys. *Thermochim. Acta* **2000**, *363*, 105–113. [CrossRef]

27.   Dai, H.; Tao, D.P. Application of the modified molecular interaction volume model (M-MIVM) to vapor-liquid phase equilibrium of binary alloys in vacuum distillation. *Vacuum* **2019**, *163*, 342–351. [CrossRef]

28.   Tao, D.P. Prediction of the coordination numbers of liquid metals. *Metall. Mater. Trans. B.* **2005**, *36*, 3495–3497. [CrossRef]

29.   Das, N.; Mittra, J.; Murty, B.S.; Pabi, S.K.; Kulkarni, U.D.; Dey, G.K. Miedema model based on methodology to predict amorphous-forming-composition range in binary and ternary systems. *J. Alloys Compd.* **2013**, *550*, 483–495. [CrossRef]

30.   Miedema, A.R.; de Châtel, P.F.; de Boer, F.R. Cohesion in alloys-fundamentals of a semi-empirical model. *Physica B+C* **1980**, *100*, 1–28. [CrossRef]

31.   Hildebrand, J.H.; Scott, R.L. *Regular Solution*; Prentiss-Hall: Hoboken, NJ, USA, 1962.

32.   Hardy, H.K. "sub-regular solution" model and its application to some binary alloy systems. *Acta. Metall.* **1953**, *1*, 202–209. [CrossRef]

33.   Alcock, C.B.; PItkin, V.; Horrigan, M.K. Vapour Pressure Equations for the Metallic Elements: 298-2500K. *Can. Metall. Q.* **1984**, *23*, 309–313. [CrossRef]

34.   Dai, Y.N.; Yang, B. *Vacuum Metallurgy of Nonferrous Metal Materials*; Metallurgical Industry Press: Beijing, China, 2000.

35.   Wang, Y.N.; Kong, L.X.; Yang, B. Simulation prediction and experimental study of phase equilibria of Bi-Sb and Bi-Sb-Cd alloys in vacuum distillation. *Vacuum* **2023**, *213*, 112032. [CrossRef]

36.   Seyf, J.Y.; Flasafi, S.M.; Babaei, A.H. Development of the NRTL functional activity coefficient (NRTL-FAC) model using high quality and critically evaluated phase equilibria data. 1. *Fluid Phase Equilibr.* **2021**, *541*, 113088. [CrossRef]

37. Wang, L.Y.; Zhao, H.; Han, L.J.; Wang, Y.F.; Xin, J.Y. Isobaric Vapor-Liquid Equilibrium of Binary Mixtures of 2-Methylpentanedioic Acid Dimethyl Ester and Dimethyl Adipate at 101.3, 50.0, 30.0, and 10.0 kPa. *J. Chem. Eng. Data* **2024**, *69*, 1613–1620. [CrossRef]
38. Liu, F.S. *Study on the Evaporative Discipline of Silver in Copper-Silver Alloys by Vacuum Distillation*; Kunming University of Science and Technology: Kunming, China, 2017.
39. Chen, Y.H.; Yang, H.W. Separation of Antimony from Copper in Vacuum Distillation. IOP Conf. *Ser. Earth Environ. Sci.* **2019**, *252*, 022035. [CrossRef]